On the Rayleigh–Bénard problem in the continuum limit

Avshalom Manela and Itzchak Frankel[a)]
Faculty of Aerospace Engineering, Technion-Israel Institute of Technology, Haifa 32000, Israel

(Received 10 March 2004; accepted 7 December 2004; published online 16 February 2005)

The transition to convection in the Rayleigh–Bénard problem at small Knudsen numbers is studied via a linear temporal stability analysis of the compressible "slip-flow" problem. No restrictions are imposed on the magnitudes of temperature difference and compressibility-induced density variations. The dispersion relation is calculated by means of a Chebyshev collocation method. The results indicate that occurrence of instability is limited to small Knudsen numbers ($\mathrm{Kn} \lesssim 0.03$) as a result of the combination of the variation with temperature of fluid properties and compressibility effects. Comparison with existing direct simulation Monte Carlo and continuum nonlinear simulations of the corresponding initial-value problem demonstrates that the present results correctly predict the boundaries of the convection domain. The linear analysis thus presents a useful alternative in studying the effects of various parameters on the onset of convection, particularly in the limit of arbitrarily small Knudsen numbers. © *2005 American Institute of Physics*.
[DOI: 10.1063/1.1861876]

I. INTRODUCTION

The onset of convection in an initially quiescent fluid confined between parallel horizontal walls and heated from below is a classical problem in hydrodynamic stability theory and has been investigated extensively owing to its relevance to free convection phenomena (see Refs. 1–3). Most studies have been carried out within the framework of the Boussinesq approximation where fluid-density variations are only considered in the buoyancy term of the equation of motion. This approximation is based on the assumptions that relative temperature differences and density variations owing to compressibility are both small. The stability problem is then governed by a single parameter, the Rayleigh number [see (17)] representing the relative effects of buoyancy, fluid viscosity, and heat conductivity.

Most of the relatively few analyses which have hitherto addressed the corresponding compressible-flow problem have relaxed either one but not both of these assumptions. Thus, Jeffreys,[4] Giterman and Shteinberg,[5] and more recently Bormann[6] considered compressibility effects assuming small temperature differences and hence constant viscosity and thermal conductivity coefficients. Frölich, Laure, and Peyret[7] studied the effects of large temperature differences while retaining the assumption that compressibility-induced density variations were negligible. In both cases the results indicate that the compressible-fluid system is less unstable than the corresponding predictions based on the Boussinesq approximation. Unlike Refs. 4–7, Spiegel[8] has apparently relaxed both of the above assumptions. His analysis, however, considers constant fluid viscosity and heat conductivity, which may not be consistent with large temperature variations. Addressing the continuum gas-dynamic problem without *a priori* restricting the relative temperature differences or compressibility-induced density variations is thus one of the main objectives of the present contribution.

The RB problem in rarefied gases has in recent years attracted considerable interest as a model problem for studying such fundamental issues as the mechanisms of instability and self-organization at the molecular level and their relation to macroscopic phenomena.[9] The two-dimensional problem has principally been studied by means of the direct simulation Monte Carlo (DSMC) method.[10–14] The numerical simulations follow the evolution of the system through its terminal state which, in turn, serves to classify the system response as stable or unstable. Early investigations[10,11] assumed an external field proportional to the prescribed temperature gradient so as to artificially retain the Boussinesq approximation depending only on the Rayleigh number. Golshtein and Elperin[12] pointed out the importance of allowing for arbitrary temperature differences and attendant compressibility effects. Consequently, they noted that the resulting problem could not be completely characterized in terms of the Rayleigh number. Sone and co-workers[15,16] considered the corresponding problem for a Bhatnagar–Gross–Krook model equation. Making use of a finite-difference scheme, they studied the effects of the Knudsen (Kn) and Froude (Fr) numbers, the temperature ratio and the geometry of the rectangular domain occupied by the gas. Stefanov and Cercignani[13] and Stefanov, Roussinov, and Cercignani[14] (hereafter referred to as SRC) studied the RB problem for a hard-sphere gas. The latter paper (SRC)[14] compares the DSMC results to those obtained via a finite-difference scheme applied to a continuum slip model. Both schemes provide closely similar results. For specific values of the temperature ratio and the aspect ratio of the rectangular fluid cell, the domain of convection in the (Fr, Kn) plane of parameters is delineated.

All of the above-mentioned studies demonstrate that significant convection only occurs at small $O(10^{-2})$ Knudsen numbers. However, the artificial "noise" inherent in DSMC

[a)]Author to whom correspondence should be addressed. Electronic mail: aeritzik@aerodyne.technion.ac.il

makes it difficult to clearly identify and characterize the final states, particularly for parameters combinations in the vicinity of the transition to convection. Furthermore, these simulations become extremely time consuming in the continuum limit, which obstruct an accurate delineation of the domain of instability. The present contribution is thus intended to avoid these difficulties and complement the above studies by considering the corresponding linear hydrodynamic temporal-stability problem in the continuum limit. Towards this end, we make use of a continuum model consisting of the Navier–Stokes equations corresponding to a monatomic hard-sphere gas. These are supplemented by the first-order velocity-slip and temperature-jump conditions corresponding to purely diffuse reflection at the walls.[9] (Higher-order slip conditions are discussed by Hadjiconstantinou.[17]) Use of this model in the context of the present RB problem is supported by the results of SRC (Ref. 14) (see the discussion in Sec. V).

In the following section we formulate the linearized perturbation problem about the pure-conduction reference state. Subsequently, in Sec. III we describe the neutral surface in the space of (Fr, Kn) and the dimensionless wave numbers. In Sec. IV we consider discrete spectra occurring for finite aspect ratios of the (rectangular) fluid domain. Finally, in Sec. V we discuss the applicability of the continuum slip model and the impact of the slip boundary conditions and make some concluding remarks.

II. STATEMENT OF THE PROBLEM

Making use of the standard normalization in studies of the RB problem in rarefied gases, the position vector is scaled by D, the distance between the walls, the gas density by the reference value $\bar{\rho}$ associated with the normalization condition (6), and the temperature is normalized by T_h, the absolute temperature of the lower (hot) wall. The transport coefficients of shear viscosity and heat conductivity are normalized by their respective values μ_h and κ_h at T_h. Fluid velocity is rendered dimensionless by the mean thermal speed $Uth=(2RT_h)^{1/2}$ (wherein R is the gas constant) and the pressure is normalized by $\bar{\rho}RT_h$.

In a compressible Newtonian fluid the dimensionless pressure, velocity, temperature, and density thus defined are governed by the continuity, Navier–Stokes, and energy equations together with the equation of state. We write these equations in a Cartesian system of coordinates (x_1,x_2,x_3) whose origin lies on the lower wall and whose x_2 axis is pointing upwards (opposite to the direction of **g**, the acceleration of gravity). In these coordinates

$$\frac{\partial \rho}{\partial t}+\frac{\partial}{\partial x_i}(\rho u_i)=0, \tag{1}$$

$$\rho\frac{Du_i}{Dt}=-\frac{1}{2}\frac{\partial p}{\partial x_i}+\mathrm{Kn}\frac{\partial}{\partial x_j}\left[2\mu\left(e_{ij}-\frac{1}{3}\frac{\partial u_j}{\partial x_i}\right)\right]-\frac{\rho}{\mathrm{Fr}}\delta_{i2}, \tag{2}$$

$$\rho\frac{DT}{Dt}=\frac{\gamma \mathrm{Kn}}{\mathrm{Pr}}\frac{\partial}{\partial x_i}\left(\kappa\frac{\partial T}{\partial x_i}\right)-(\gamma-1)p\frac{\partial u_i}{\partial x_i}+2(\gamma-1)\mathrm{Kn}\Phi, \tag{3}$$

and

$$p=\rho T. \tag{4}$$

In the above summation of repeated indices is implied, D/Dt denotes the material derivative and δ_{ij} is the Kronecker delta. Appearing in (2) and (3) are the rate-of-strain tensor $e_{ij}=(\partial u_i/\partial x_j+\partial u_j/\partial x_i)/2$ and the rate of dissipation $\Phi=2\mu(e_{ij}e_{ij}-(\partial u_i/\partial x_i)^2/3)$. The dimensionless parameters appearing in the equations are the Knudsen number, $\mathrm{Kn}=l/D$, representing the ratio of l, the mean free path and the macroscopic scale D; the Froude number, $\mathrm{Fr}=U_{th}^2/gD$, describing the relative magnitudes of gas inertia and gravity; the Prandtl number, $\mathrm{Pr}=\mu_h c_p/\kappa_h$ and $\gamma=c_p/c_v$, the ratio of specific heats at constant pressure and volume, respectively. We consider a monatomic hard-sphere gas. For this model of molecular interaction $\gamma=5/3$ and $\mathrm{Pr}=2/3$. In addition, the Chapman–Enskog scheme[18] yields for the leading order of the dimensionless transport coefficients

$$\mu(T)=\kappa(T)=\frac{5\pi^{1/2}}{16}T^{1/2}. \tag{5}$$

The above equations are supplemented by the normalization condition

$$\int \rho \mathrm{d}x_1\mathrm{d}x_2\mathrm{d}x_3=1, \tag{6}$$

specifying the total amount of gas between the walls, and by the boundary conditions

$$u_2=0,\quad u_{1,3}=\zeta\frac{\partial u_{1,3}}{\partial x_2},\quad T=1+\tau\frac{\partial T}{\partial x_2}\quad \text{at } x_2=0, \tag{7}$$

$$u_2=0,\quad u_{1,3}=-\zeta\frac{\partial u_{1,3}}{\partial x_2},\quad T=R_T-\tau\frac{\partial T}{\partial x_2}\quad \text{at } x_2=1, \tag{8}$$

respectively, imposing the vanishing of the normal velocity component and specifying the magnitudes of velocity slip and temperature jump at the lower ($y=0$) and upper ($y=1$) walls. In (7) and (8), $R_T=T_c/T_h$ denotes the ratio of cold- and hot-wall temperatures, $\zeta=1.1466\mathrm{Kn}$ and $\tau=2.1904\mathrm{Kn}$.[9]

SRC (Ref. 14) obtained for the above problem the steady "pure conduction" (i.e., $u_i^{(0)}=0$) solution

$$T^{(0)}=(Ax_2+B)^{2/3},\quad \rho^{(0)}=\frac{C}{T^{(0)}}\exp\left[-\frac{6}{A\mathrm{Fr}}T^{(0)^{1/2}}\right], \tag{9}$$

in which the constants A, B, and C are determined by use of (6)–(8). The linear temporal stability of this pure-conduction reference state is analyzed by assuming that it is perturbed by small spatially harmonic perturbations. Accordingly, each of the above-mentioned fields is generically represented by the sum

$$F = F^{(0)}(x_2) + \phi^{(1)}(x_2)\exp[i\mathbf{k}\cdot\mathbf{r} + \omega t], \tag{10}$$

wherein $F^{(0)}$ denotes the steady reference state and $\mathbf{k}=(k_1,k_3)$ and $\mathbf{r}=\mathbf{r}(x_1,x_3)$ are, respectively, the wave number vector and the position vector in the (x_1,x_3) plane parallel to the walls. The above problem is transversely symmetric about the x_2 axis. We may therefore, with no loss of generality, confine subsequent description to vertical planes parallel to $\mathbf{k}$. To simplify notation we thus select the x-axis parallel to $\mathbf{k}$ and rewrite u_1, u_2, and x_2 as u, v, and y, respectively. Substituting (10) into (1)–(3), neglecting nonlinear terms and eliminating the pressure p by use of the equation of state (4), we obtain in the new notation the perturbation problem consisting of

$$\omega\rho^{(1)} + \frac{d\rho^{(0)}}{dy}v^{(1)} + \rho^{(0)}\left[\frac{dv^{(1)}}{dy} + f^{(1)}\right] = 0, \tag{11}$$

$$\omega\rho^{(0)}f^{(1)} = \frac{1}{2}k^2[\rho^{(0)}T^{(1)} + \rho^{(1)}T^{(0)}] + \mathrm{Kn}\left\{\frac{d\mu^{(0)}}{dy}\left[\frac{df^{(1)}}{dy} - k^2v^{(1)}\right] + \mu^{(0)}\left[\frac{d^2f^{(1)}}{dy^2} - \frac{k^2}{3}\left(\frac{dv^{(1)}}{dy} + 4f^{(1)}\right)\right]\right\}, \tag{12}$$

$$\omega\rho^{(0)}v^{(1)} = -\frac{1}{2}\frac{d}{dy}[\rho^{(0)}T^{(1)} + \rho^{(1)}T^{(0)}] + \mathrm{Kn}\left\{\frac{d\mu^{(0)}}{dy}\left[\frac{4}{3}\frac{dv^{(1)}}{dy} - \frac{2}{3}f^{(1)}\right] + \mu^{(0)}\left[\frac{4}{3}\frac{d^2v^{(1)}}{dy^2} + \frac{1}{3}\frac{df^{(1)}}{dy} - k^2v^{(1)}\right]\right\} - \frac{1}{\mathrm{Fr}}\rho^{(1)}, \tag{13}$$

and

$$\omega\rho^{(0)}T^{(1)} + \rho^{(0)}v^{(1)}\frac{dT^{(0)}}{dy} = -\frac{2}{3}\rho^{(0)}T^{(0)}\left[\frac{dv^{(1)}}{dy} + f^{(1)}\right] + \frac{5}{2}\mathrm{Kn}\left\{\frac{d\kappa^{(0)}}{dy}\frac{dT^{(1)}}{dy} + \frac{dT^{(0)}}{dy}\frac{d\kappa^{(1)}}{dy} + \kappa^{(0)}\left[\frac{d^2T^{(1)}}{dy^2} - k^2T^{(1)}\right] + \kappa^{(1)}\frac{d^2T^{(0)}}{dy^2}\right\}, \tag{14}$$

wherein $f^{(1)}=iku^{(1)}$. These equations are supplemented by the boundary conditions

$$f^{(1)} = \pm\zeta\frac{df^{(1)}}{dy}, \quad v^{(1)} = 0, \quad T^{(1)} = \pm\tau\frac{dT^{(1)}}{dy} \tag{15}$$

at $y=0,1$, respectively. In (12)–(14), $\mu^{(0)}=\kappa^{(0)}=(5\pi^{1/2}/16)T^{(0)^{1/2}}$ and $\kappa^{(1)}=(5\pi^{1/2}/32)T^{(0)^{-1/2}}T^{(1)}$, in accordance with linearization of (5). The assumed form (10) ensures that $\rho^{(1)}$ satisfies the homogeneous equivalent of (6).

The dispersion relation $\omega=\omega(k;\mathrm{Kn},\mathrm{Fr},R_T)$ is calculated by means of the Chebyshev collocation method.[19] This method transforms the above problem into an algebraic eigenvalue problem consisting of a system of $4N$ linear equations satisfied by the perturbations $\rho^{(1)}$, $f^{(1)}$, $v^{(1)}$, and $T^{(1)}$ at N discrete points across the gas domain. Throughout the domain of parameters corresponding to subsequent results, convergence of the calculation is established within $N<70$. In particular, unlike DSMC computations, there is no difficulty in obtaining results for arbitrarily small $\mathrm{Kn}>0$.

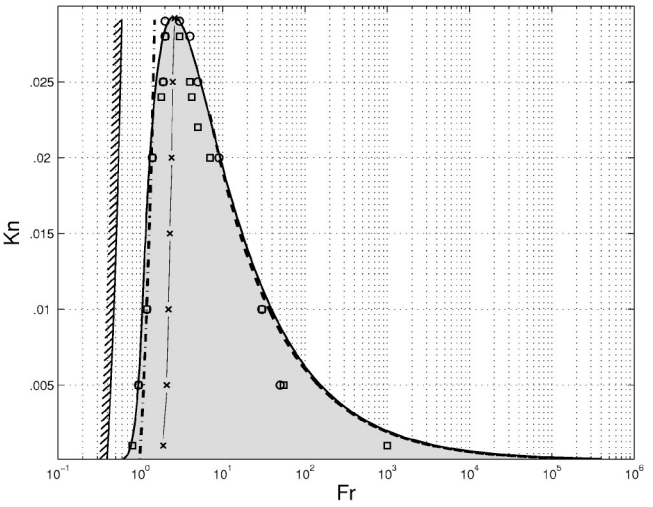

FIG. 1. Division of the plane of parameters (Fr, Kn) into unstable (U, shaded zone) and stable (S) domains for $R_T=0.1$ according to the present linear theory (solid line) together with DSMC (circles) and continuum (squares) results of SRC (Ref. 14). Also marked are the large-Fr asymptote $\mathrm{Ra}_m\approx 1773$ (dashed line), the locus of perturbations possessing the largest growth rates at given Kn (crosses joined by line segments), the initial appearance of nonmonotonical density distribution (dash-dotted line), and the necessary condition (18) for the onset of convection (cross-hatched line).

III. RESULTS AND DISCUSSION

Throughout the entire domain of parameters our calculations invariably yield real-valued ω. Accordingly, the onset of convection takes place via "exchange of stabilities,"[1] i.e., the appearance of stationary perturbations, $\omega=0$. In the following we focus on a temperature ratio $R_T=0.1$ so as to facilitate comparison with the results of SRC.[14]

The solid line in Fig. 1 separates the plane of parameters (Fr, Kn) into respective domains of unstable (U, shaded zone), $\omega>0$, and stable (S), $\omega<0$, response. Also presented are the corresponding DSMC (circles) and continuum finite-difference (squares) results of SRC,[14] the large-Fr asymptote ($\mathrm{FrKn}^2\approx 3.65\times 10^{-3}$, dashed line), the dash-dotted line marking the locus of states where nonmonotonical density distributions initially appear in the pure-conduction reference state (9) and the cross-hatched line corresponding to the necessary condition (18) related to compressibility-induced density variations. Finally, the crosses joined by the line segments mark the points where, according to the present linear analysis, perturbations possess maximal growth rates for respectively given values of Kn.

For all $\mathrm{Kn}>0$ the convection domain is confined to a finite interval of Froude numbers. The extent of this interval is rapidly diminishing with increasing Kn, vanishing entirely for $\mathrm{Kn}\gtrsim 0.029$. When $\mathrm{Kn}\lesssim 0.01$ (and $\mathrm{Fr}\gtrsim 40$), the right branch of the U-domain boundary is approaching the dashed

line. The latter corresponds to the modified Rayleigh number based on the arithmetic mean of wall temperatures

$$\mathrm{Ra}_m = \frac{2048}{75\pi(1+R_T)^2}\frac{1-R_T}{\mathrm{FrKn}^2} \approx 1773 \tag{16}$$

(cf. Golshtein and Elperin[12]). In the limit when the temperature difference is small this expression reduces to the traditional expression

$$\mathrm{Ra} = \frac{g(1-R_T)D^3\rho^2 c_P}{\mu\kappa}. \tag{17}$$

The coincidence of the $\mathrm{Fr} \gg 1$ portion of the *U*-domain boundary with a critical value of Ra_m which is larger than the Boussinesq value (≈ 1708) is in agreement with the results of Frölich *et al.*[7] who studied this limit within the framework of the Low–Mach approximation of the Navier–Stokes equations. Thus, according to Frölich *et al.*,[7] the critical value of Ra_m is growing with increasing relative temperature differences essentially owing to the variation of the transport coefficients (μ and κ) with the local gas temperature (which effect is neglected in the Boussinesq approximation). This correspondence of the lower-right boundary with a constant critical value of Ra_m would not occur in the presence of significant compressibility effects (i.e., density variations resulting from pressure differences). However, when $\mathrm{Fr} \gg 1$, the pressure is nearly uniform across the fluid domain [cf. (9)], hence $\rho \approx \rho(T)$ and compressibility effects are indeed negligible.

We now turn to consider the left branch of the *U*-domain boundary. It is interesting to note that for all $\mathrm{Kn} \lesssim 0.02$, this boundary is disposed to the left of the dash-dotted line. Indeed, transition to convection may take place in a compressible fluid even when the fluid density in the reference state is monotonically decreasing.[6] Thus, convection may set in provided that adiabatic expansion of a fluid element rising through the reference hydrostatic pressure field reduces its density below the ambient reference density.[20] In the present dimensionless notation, this yields the condition

$$\Delta(y) = \frac{dT^{(0)}}{dy} + \frac{4}{5\mathrm{Fr}} < 0. \tag{18}$$

The cross-hatched line in the figure presents the locus of conditions where (18) is initially satisfied by the reference fluid-temperature gradient. From (9) we see that this condition initially occurs at the upper (cold) wall.[21] The analysis leading to (18) does not consider the retarding effects of fluid viscosity and heat conductivity, hence this condition is in fact a necessary condition for the onset of convection. As such, it is not surprising that the corresponding line appears to the left of the actual boundary. We further elaborate on the relevance of (18) towards the conclusion of this section.

In view of the vastly different methods of calculation (a linearized eigenvalue problem as opposed to a nonlinear initial value problem), the close agreement between the present results and those of SRC (Ref. 14) is gratifying. The largest differences between the respective results appear at the lower portion of the right branch of the boundary ($\mathrm{Kn} \lesssim 0.01, \mathrm{Fr} \gg 1$) of the convection domain which is wider according to

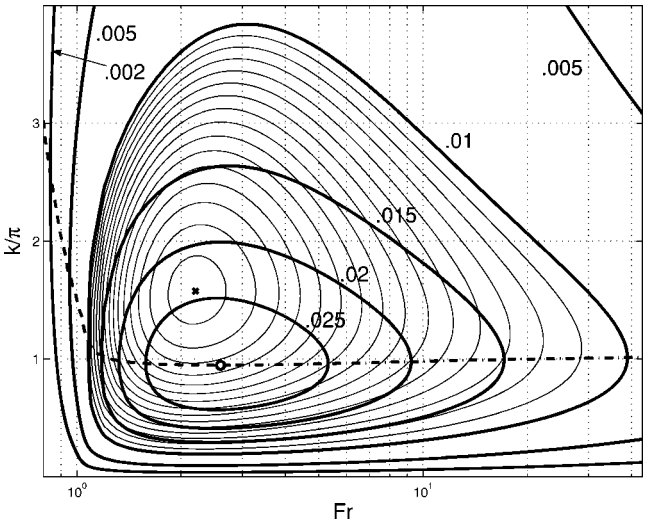

FIG. 2. A "top view" of the neutral surface $\omega(\mathrm{Fr},\mathrm{Kn},k)=0$ over the (Fr,k) plane for $R_T=0.1$. Neutral curves at the indicated values of Kn are marked by the bold solid lines. Thin solid lines are level lines of ω for $\mathrm{Kn}=0.01$ ($\Delta\omega=0.02$). The dashed and dash-dotted curves joined by the circle describe the projection of the neutral curve (bold solid line) in Fig. 1 on the (Fr,k) plane.

the present results. This difference may be attributed to nonlinear (hysteresis) phenomena (which are obviously absent from the present linear analysis). For example, consider the location of the right boundary at $\mathrm{Kn}=0.005$. The corresponding values of the Froude number are $\mathrm{Fr} \approx 152$ in the present calculation and $\mathrm{Fr} \approx 50-55$ in SRC.[14] However, their Fig. 12 shows wide hysteresis loop extending as far as $\mathrm{Fr} \approx 200$. Thus, in this part of the (Fr, Kn) plane the convection domain is bounded by a zone rather than a line; the boundary delineated by the present linear calculation is passing through this zone. Traversing the rest of the boundary of the *U* domain we observe that in its upper ($\mathrm{Kn} \gtrsim 0.02$) portion the differences between the present line and the results of SRC (Ref. 14) are comparable to the differences between their various schemes. At the lower-left portion of the boundary [$\mathrm{Kn} \lesssim 0.02, \mathrm{Fr} \approx O(1)$] the results of all calculations nearly coincide. Similarly to the above, this correspondence is in accordance with the hysteresis loops here being much narrower than those encountered on the right branch of the bounding curve [cf. Figs. 11 and 12 of SRC (Ref. 14)].

Figure 2 describes a "top view" of the three-dimensional neutral surface $\omega(k;\mathrm{Fr},\mathrm{Kn})=0$ (for $R_T=0.1$) above the plane of Fr and k, the dimensionless wave number, which thus complements the "front view" of the preceding figure. The bold solid lines are the neutral curves ($\omega=0$) at the indicated values of Kn. With increasing Kn, the extent of the *U* domain is rapidly diminishing. Also presented for $\mathrm{Kn}=0.01$ are the level lines of the growth rate (the separation between adjacent lines being $\Delta\omega=0.02$). The local maximum of the growth rate ($\omega_m \approx 0.309$) is marked by the cross at $k \approx 4.95$, $\mathrm{Fr} \approx 2.20$ (corresponding to the cross marked at $\mathrm{Kn}=0.01$ in Fig. 1). Noting that Fr values are described on a logarithmic scale, we see that the larger growth rates occur in the proximity of the left (small Fr) boundary of the *U* domain (cf. the crosses marked in Fig. 1).

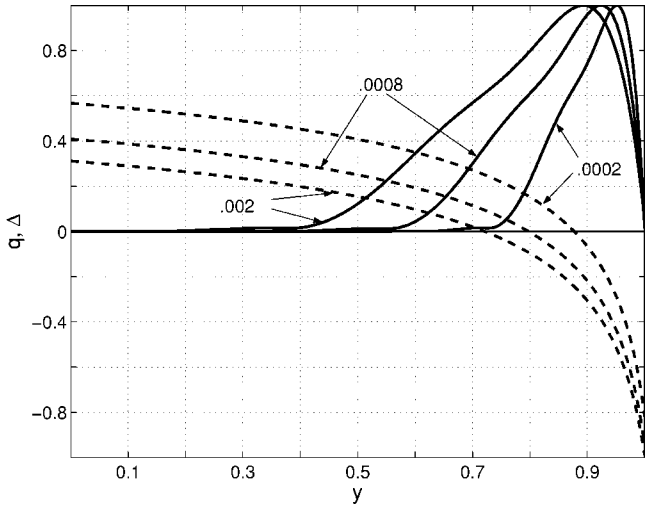

FIG. 3. The variation across the fluid domain of $q(y)$, the x average of convection intensity, (solid line), and $\Delta(y)$, associated with the necessary condition (18) (dashed lines) at the indicated values of Kn.

The projection of the neutral curve of Fig. 1 on the (Fr, k) plane is described by the combination of the dash-dotted (right branch) and dashed (left branch) lines joined at the bold circle (peak). At each point of the neutral curve of Fig. 1 the present line gives the corresponding dimensionless wave number k_{cr}. For future reference we note that throughout the entire right branch as well as in the upper portion ($\mathrm{Kn}\gtrsim 0.02, \mathrm{Fr}\gtrsim 1.23$) of the left branch only slight changes from $k_{cr}\approx\pi$ appear. With further decreasing Fr and Kn, k_{cr} veers up and becomes rapidly increasing. Finally, we observe that the curvature of the neutral curves about their respective intersections with the k_{cr} line is decreasing with diminishing Fr and Kn. Consequently, in the vicinity of these intersections a slight increase of Fr is sufficient to render unstable a wide spectrum of perturbation wave numbers.

To gain some further insight into the effects of compressibility, we focus on the lower left portion of the U-domain boundary. Towards this end, we consider the variation across the gas domain of $\Delta(y)$ [see (18)] and $q(y)$, the x average of convection intensity (normalized to unity). These are presented in Fig. 3 by the respective dashed and solid lines at the indicated Knudsen numbers corresponding to three points on the lower left branch of the neutral curve of Fig. 1.

It may readily be established that $\Delta(y)$ is monotonically decreasing. Furthermore, $|dT^{(0)}/dy|$ is decreasing with Kn tending to increase Δ. However, at the small values of Kn concerned (0.0002–0.002) this has only a slight effect which is dominated by the diminishing of the second term as we move along the neutral curve to larger values of Fr (specifically from $\mathrm{Fr}\approx 0.66$ to $\mathrm{Fr}\approx 0.84$). Consequently, with increasing Fr and Kn, $\Delta(y)$ decreases and the interval δ_1 adjacent to the cold wall where the necessary condition (18) is satisfied is widening.

At $\mathrm{Kn}=0.0002$ convection is effectively confined to the upper quarter of the gas domain. With increasing (Kn, Fr) this convection zone δ_2 is growing so that its extent is a little more than twice that of the corresponding δ_1. This correlation remains valid with very slight deviations up to $\mathrm{Kn}\approx 0.005$ when convection nearly occupies the entire gas domain between the walls. These results appear to agree qualitatively with Figs. 2 and 3 in SRC.[14]

The foregoing discussion demonstrates the usefulness of (18) to the rationalization of the onset of convection under significant compressibility effects and temperature differences. Being a necessary condition (which neglects retarding viscous and heat-conduction effects) it is insufficient to require $\Delta(1)<0$ at the upper cold wall (see the cross-hatched line in Fig. 1). Rather (depending on Fr, Kn) there is a threshold critical interval δ_1 where (18) needs to be satisfied before convection may be sustained. Once convection sets in it extends over a wider (than δ_1) portion of the gas domain δ_2 owing to viscous momentum diffusion to lower fluid layers.

IV. DISCRETE SPECTRA

Existing studies of RB instability in rarefied gases consider two-dimensional problems in rectangular domains. Periodicity[14] or specular reflection[10–13,15,16] conditions are imposed at the vertical planar boundaries (perpendicular to the walls at $x=0,L$). The finite domain together with the boundary conditions prescribed result in a discrete spectrum of perturbation wavelengths. Thus, for a cell whose aspect ratio is $R_L=L/D$ with periodicity condition, the dominant perturbations need to be selected from the discrete set of wave numbers $k_n^{(d)}=2\pi n/R_L$ $(n=1,2,\ldots)$. These, in turn, correspond to occurrence of n pairs of convection rolls within the rectangular domain.[22]

The transition from a continuous spectrum to a discrete subset of perturbation wave numbers is expected to diminish the U-domain. We here focus on a cell whose aspect ratio is $R_L=2$, as in SRC.[14] For this value of R_L our calculations show that the actual displacement of the neutral curve is imperceptible in Fig. 1. This result may be rationalized by considering the projection of the neutral curve presented in Fig. 2. As mentioned above, throughout the right branch and the upper portion of the left branch the "continuous" critical wave numbers deviate only slightly from $k_{cr}\approx\pi$. Selection of the discrete counterpart $k_{cr}^{(d)}=\pi$ $(n=1)$ thus results in slight (indiscernible) changes of the critical Fr value corresponding to a given Kn. Different values of R_L may, however, result in a more significant diminution of the U domain. Regarding the left branch of the U-domain boundary, it has been observed in Fig. 2 that for a given pair of (Fr, Kn) $\omega\approx 0$ within a wide interval of wave numbers about k_{cr}. Thus, the lower left branch too is only slightly modified as a result of replacing k_{cr} by the appropriate discrete value $k_{cr}^{(d)}$. Unlike the right branch of the neutral curve, this result is less sensitive to the specific value of R_L.

The discrete counterpart of the k_{cr} curve presented in Fig. 2 is obtainable through comparison of the respective Fr values corresponding to $\omega=0$ for the various discrete modes $k_n^{(d)}$ at a given Kn. Thus $k_{cr}^{(d)}=\pi$ throughout the right branch and the upper $\mathrm{Kn}\gtrsim 0.0066$ part of the left branch. For $0.0021\lesssim\mathrm{Kn}\lesssim 0.0066$ $k_{cr}^{(d)}=2\pi$ would prevail and for $0.000\,83\lesssim\mathrm{Kn}\lesssim 0.0021$ $k_{cr}^{(d)}=3\pi$. When Kn is further reduced $k_{cr}^{(d)}$ increases. These results are compatible with the

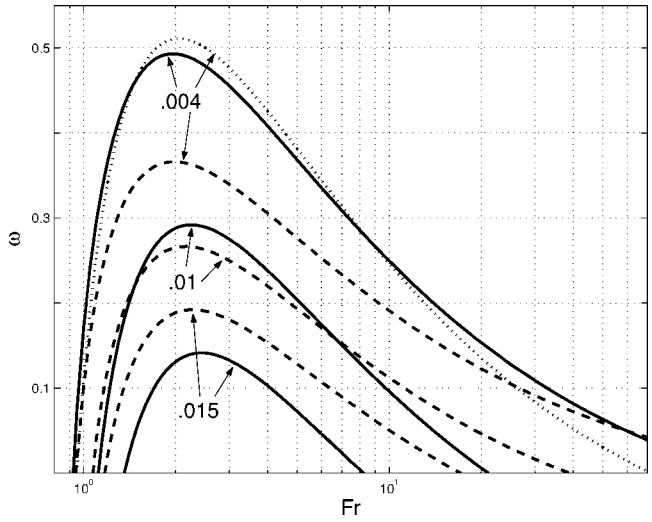

FIG. 4. The dominant discrete modes in a rectangular domain $L/D=2$ for $R_T=0.1$ and the indicated Knudsen numbers; $k=\pi$ (dashed), 2π (solid), and 3π (dotted).

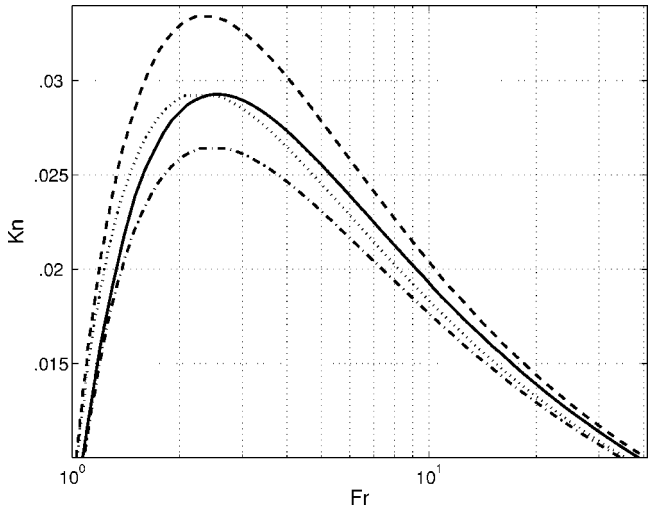

FIG. 5. Comparison of the present neutral curve (solid line) and those obtained in the absence of velocity slip (dash dotted), temperature jump (dashed), and both (dotted).

(even) numbers of convection rolls at points on the lower-left boundary of the convection zone tabulated in SRC.[14]

As mentioned above, linear stability analysis is also concerned in determining the dominant perturbations, i.e., those possessing the maximal growth rate for a given set of parameters. To clarify the effects of Kn and Fr on the selection of the dominant discrete perturbations, Fig. 4 describes the variation of ω with Fr for the dimensionless wave numbers $k=\pi$ (dashed lines), 2π (solid curves), and 3π (dotted line) at the indicated values of Kn. At the largest value of Kn (=0.015) presented, the basic wave number $k=\pi$ is the dominant mode for all Fr (which remains true for $\mathrm{Kn}\gtrsim 0.011$). With decreasing Kn, an increasing number of higher-order modes emerge as dominant perturbations, initially appearing near $\mathrm{Fr}\approx 2$ (in the vicinity of the maximal ω for a given Kn, cf. the crosses marked in Fig. 1). While the number of bifurcations is rapidly increasing they become more gradual in the sense that the modes involved possess comparable growth rates over larger Fr intervals. This may affect the weakly nonlinear behavior of perturbations by modifying, at small Kn, the assumed exponential time dependence (10). Finally, in accordance with the above discussion of k_{cr}, for all Kn and sufficiently large Fr (i.e., when approaching the right boundary of the U domain), the dominant perturbation corresponds to the basic harmonic $k=\pi$.

V. CONCLUDING REMARKS

Evaluation of the validity and accuracy of the present results is closely related to the prediction of the failure of the continuum slip-flow model employed. Earlier Refs. 23 and 24 require that $\mathrm{Kn}\lesssim 0.1$, which condition is apparently satisfied since the present results indicate that the onset of convection only takes place when $\mathrm{Kn}\lesssim 0.03$. However, the foregoing is an overall Knudsen number involving the mean free path l based on the average density $\bar{\rho}$ and the global macroscale D. Criteria based on the smallness of such average Knudsen numbers may not be uniformly valid and may locally fail at certain parts of the flow field.[25,26] A more careful examination of this issue involves a local Knudsen number based on the local mean free path and an appropriate local macroscopic scale. The latter may be defined in terms of some macroscopic field Q and its local gradients, i.e., $Q/|\nabla Q|$. However, there is no unique commonly accepted failure criterion. Rather, varying forms and upper bounds of the local Knudsen number appear in the literature in the context of different physical problems.[26–29] The ultimate test in any case is based on the comparison of the continuum model predictions to DSMC results. For the RB problem, the comprehensive comparison which has been carried out by SRC (Ref. 14) has demonstrated good agreement between the respective results of both schemes throughout the relevant domain of parameters. This agreement ensures adequacy of the present model which (apart from the linearization of the perturbation equations) is the same as the continuum model of SRC.[14]

To examine the influence of the velocity-slip and temperature-jump boundary conditions (7) and (8), respectively, on the stability of the system, Fig. 5 compares the present neutral curve (solid line) to the one obtained when the vanishing of velocity slip [$\zeta=0$ in (7) and (8)] and temperature jump [$\tau=0$ in (7) and (8)] are imposed (dotted curve). Also presented are the boundaries of the U domain obtained in the absence of either velocity slip (dash-dotted curve) or temperature jump (dashed curve). The various curves converge with diminishing Kn, hence we focus on their respective upper ($\mathrm{Kn}\gtrsim 0.01$) parts.

There is a relatively small difference between the solid and dotted lines—a slight leftward shift of the latter. The present solution thus predicts a somewhat wider convection domain at larger Fr (i.e., the right branch) and somewhat more stable response at small Fr (the left branch). The remaining curves demonstrate that the foregoing small difference results from the summation of two mutually opposing effects. Thus, on the one hand, the no-slip condition effectively enhances the retarding effect of fluid viscosity. On the

other hand, the absence of temperature jump at the walls increases (for a given temperature ratio) the actual temperature gradient across the fluid and thus enhances the destabilizing effect of buoyancy. The former is more significant at the larger Fr values, increasing the critical value of Ra_m required for the onset of convection. The latter mainly affects the left boundary of the U domain by advancing the satisfaction of (18) at smaller Fr. While each of these would separately yield a relatively substantial change, together they nearly cancel each other.

The present linear temporal stability analysis focuses on the onset of convection in RB problem in the continuum limit. The above discussion indicates that the boundaries of the domain of instability are essentially determined by two factors: (i) The increasing of the critical Rayleigh number related to variation of fluid viscosity and heat conductivity with temperature and (ii) the cutoff at finite $[O(1)$ for the present selection of $R_T]$ values of Fr owing to compressibility. It is the intersection of these two which results in the vanishing of RB instability beyond the relatively small Kn ≈ 0.03.

In accordance with the goals set in the Introduction, much of the discussion have been devoted to the comparison of the present results and those obtained in the nonlinear calculations of SRC.[14] Obviously, the present scheme is not expected to predict the form and intensity of the final convection patterns which are governed by nonlinear interactions. However, as demonstrated in Fig. 1, the linear analysis does successfully predict the boundary of the convection domain (associated with stationary, nongrowing perturbations which are therefore not necessarily inconsistent with the basic assumptions of the linear theory). This result offers the linear temporal stability analysis as a viable means of studying the effects of the various parameters on the onset of convection. While the present selection of $R_T=0.1$ and a hard-sphere gas was motivated by the need to facilitate comparison with SRC,[14] there is evident interest in examining, among other things, the effect of other values of R_T or alternative models of molecular interaction.

[1] S. Chandrasekhar, *Hydrodynamic and Hydromagnetic Stability* (Clarendon, Oxford, 1961).
[2] P. Drazin and W. Reid, *Hydrodynamic Stability* (Cambridge University Press, Cambridge, 1981).
[3] E. Koschmieder, *Bénard Cells and Taylor Vortices* (Cambridge University Press, Cambridge, 1993).
[4] H. Jeffreys, "The instability of a compressible fluid heated below," Proc. Cambridge Philos. Soc. **26**, 170 (1930).
[5] M. Giterman and V. Shteinberg, "Criteria of occurence of free convection in a compressible viscous heat-conducting fluid," J. Appl. Math. Mech. **34**, 305 (1970).
[6] A. Bormann, "The onset of convection in Rayleigh–Bénard problem for compressible fluids," Continuum Mech. Thermodyn. **13**, 9 (2001).
[7] J. Frölich, P. Laure, and R. Peyret, "Large departures from Boussinesq approximation in the Rayleigh–Bénard problem," Phys. Fluids A **4**, 1355 (1992).
[8] E. A. Spiegel, "Convective instability in a compressible atmosphere. I," Astrophys. J. **141**, 1068 (1965).
[9] C. Cercignani, *Rarefied Gas Dynamics* (Cambridge University Press, Cambridge, 2000).
[10] T. Watanabe, H. Kaburaki, and M. Yokokawa, "Simulation of a two-dimensional Rayleigh–Bénard system using the direct simulation Monte Carlo method," Phys. Rev. E **49**, 4060 (1994).
[11] C. Robinson and J. Harvey, "Two-dimensional DSMC calculations of the Rayleigh–Bénard instability," in *Rarefied Gas Dynamics*, edited by C. Shen (Peking University Press, Beijing, 1997), p. 168.
[12] E. Golshtein and T. Elperin, "Convective instabilities in rarefied gases by direct simulation Monte Carlo method," J. Thermophys. Heat Transfer **10**, 250 (1996).
[13] S. Stefanov and C. Cercignani, "Monte Carlo simulation of Bénard's instability in a rarefied gas," Eur. J. Mech. B/Fluids **11**, 543 (1992).
[14] S. Stefanov, V. Roussinov, and C. Cercignani, "Rayleigh–Bénard flow of a rarefied gas and its attractors. I. Convection regime," Phys. Fluids **14**, 2255 (2002).
[15] Y. Sone, K. Aoki, H. Sugimoto, and H. Motohashi, "The Bénard problem of rarefied gas dynamics," in *Rarefied Gas Dynamics*, edited by J. Harvey and G. Lord (Oxford University Press, Oxford, 1995), Vol. 1, p. 135.
[16] Y. Sone, K. Aoki, and H. Sugimoto, "The Bénard problem for a rarefied gas: Formation of steady flow patterns and stability of array of rolls," Phys. Fluids **9**, 3898 (1997).
[17] N. Hadjiconstantinou, "Comment on Cercignani's second-order slip coefficient," Phys. Fluids **15**, 2352 (2003).
[18] S. Chapman and T. Cowling, *The Mathematical Theory of Non-Uniform Gases*, 3rd ed. (Cambridge University Press, Cambridge, 1970).
[19] R. Peyret, *Spectral Methods for Incompressible Viscous Flow* (Springer, New York, 2002).
[20] L. Landau and E. Lifshitz, *Fluid Mechanics* (Pergamon, Reading, MA, 1959).
[21] In fact, since $T^{(0)}(y)$ is monotonically decreasing, this could readily be established from (3) for an arbitrary monotonically increasing $\kappa(T)$.
[22] When specular reflection is imposed the basic wavelength is twice the domain length and $k_n^{(d)}=\pi n/R_L$ $(n=1,2,\ldots)$. The nth harmonic then corresponds to n convection rolls.
[23] K. Stewartson, *The Theory of Laminar Boundary Layers in Compressible Fluids* (Clarendon, Oxford, 1964).
[24] S. Schaaf and P. Chambré, *Flow of Rarefied Gases* (Princeton University Press, Princeton, 1961).
[25] G. Bird, *Molecular Gas Dynamics and the Direct Simulations of Gas Flows* (Clarendon, Oxford, 1994).
[26] I. Boyd, "Predicting breakdown of the continuum equations under rarefied flow conditions," in *Rarefied Gas Dynamics*, edited by A. D. Ketsdever and E. P. Muntz (American Institute of Physics, New York, 2003), p. 899.
[27] I. Boyd, G. Chen, and G. Candler, "Predicting failure of the continuum fluid equations in transitional hypersonic flows," Phys. Fluids **7**, 210 (1995).
[28] A. Garcia, J. Bell, W. Crutchfield, and B. Alder, "Adaptive mesh and algorithm refinement using direct simulation Monte Carlo," J. Comput. Phys. **152**, 134 (1999).
[29] G. Bird, "Breakdown of translational and rotational equilibrium in gaseous expansions," AIAA J. **8**, 1998 (1970).